SIMULATION OF ELASTIC WAVE PROPAGATION IN MODELS CONTAINING IRREGULAR INTERFACES PARAMETERIZED ON IRREGULAR GRIDS

Bertram Nolte

Earth Resources Laboratory
Department of Earth, Atmospheric, and Planetary Sciences
Massachusetts Institute of Technology
Cambridge, MA 02139

ABSTRACT

Thus study demonstrates the advantages of a recently-developed irregular-grid modeling technique (Nolte, 1996). This technique can model irregular interfaces more accurately than a standard regular-grid finite-difference method. I show this by comparison of both methods for a simple model containing a sloping interface. While the discrete approximation to the sloping interface results in numerical inaccuracies for the finite-difference method, the irregular-grid technique produces superior results. I then show that the method can also be applied to a free surface with irregular topography, suggesting that it may be a valuable alternative to existing finite-difference free-surface algorithms.

INTRODUCTION

It is well known that finite-difference techniques (e.g., Alford *et al.*, 1974; Virieux, 1984, 1986) suffer from inaccuracies in modeling irregular interfaces, due to their discrete approximation to the model. For example, a dipping interface has to be approximated by discrete steps. This approximation can result in diffractions from these "stair steps" (Muir *et al.*, 1992). While these diffractions can often be eliminated by an isotropic interpolation of the medium parameters across the interface, more severe problems occur when larger impedance contrasts are present at an interface. Muir *et al.* (1992) presented an effective-medium approach to model irregular interfaces. Even though there is no rigorous theoretical justification for their approach, their numerical results show that it works well in cases where isotropic interpolation fails. Their method is limited to interfaces with solid material on either side, and thus cannot be applied to an irregular free surface.

Incorporating surface topography into finite-difference modeling codes has been the subject of various previous investigations (e.g., Jih *et al.* 1988; Hestholm and Ruud, 1994; Robertsson, 1996). As shown by Robertsson (1995), various methods have different shortcomings. For example, grid-distortion techniques (Tessmer *et al.*, 1992; Hestholm and Ruud, 1994; Hestholm, 1996) become unstable at steep slopes. Imaging techniques (Levander, 1988; Robertsson, 1996) appear to be more flexible in handling irregular topography. However, Robertsson (1996) was forced to use a very fine gridding in order to avoid the stair-step problems, which he found to be more severe for a free surface than for a solid-solid interface. Thus an accurate representation of an irregular free surface is computationally expensive, and alternative modeling schemes are desirable. One approach could be rectangular variable grid methods (Jastram and Tessmer, 1994; Wang and Schuster, 1996; De Lilla, 1997) combined with Robertsson's free surface algorithm. This would allow the fine gridding to be restricted to the near-surface region, while coarser gridding could be used in other parts of the model.

Here, I show an alternative method to incorporate surface topography. An irregular-triangular-grid method is presented in Nolte (1996) which is based on a finite-volume approximation (e.g., Vinokur, 1989) to the wave equation. This method allows the grid itself to be distorted so that grid points can be positioned directly on interfaces. Also, it deals with an irregular free surface the same way as with an irregular solid-solid interface, which is an advantage over the technique of Muir *et al.* (1992).

In this paper, I demonstrate the usefulness of this method with two numerical examples. First, I compare the irregular-grid technique for a model containing a sloping interface with a regular finite-difference code, and show that the former can model this case more accurately than the latter. I then present a numerical example that shows how the technique can be applied to a model with an irregular free surface.

THE MODELING TECHNIQUE

I have described the details of the technique in the previous consortium report (Nolte, 1996) and will thus only review the essentials. As there was an error in the P-SV formulation in the previous paper, I give the correct P-SV equations in the appendix. The method essentially amounts to a discrete approximation to the wave equation in integral form, while the constitutive relation is approximated in finite-difference form. The model is parameterized on a triangular Delaunay grid and its dual Dirichlet grid (see the appendix and Figure A-2 for the definition of these terms). As the Delaunay grid can be irregular, grid points can be placed directly on an interface. In my irregular-grid technique the medium parameters (λ, μ and ρ) are defined to be constant within each triangular grid cell (see Figure A-2). Thus, if grid points are positioned exactly on an interface, the two media will be separated exactly by the interface. In contrast, finite-difference implementations usually approximate the model parameters in an area around the grid point itself, which in staggered-grid techniques does not clearly define the exact position of an interface.

As stated above, the free surface is treated the same way as any other interface. On all other model boundaries, I use Higdon's (1986, 1987) absorbing boundary condition. Refer to Nolte (1996) for details of the implementation of this boundary condition on a triangular grid. So far, only a first-order absorbing boundary condition has been implemented.

COMPARISON WITH FINITE DIFFERENCE FOR A DIPPING INTERFACE

In order to test the performance of the irregular-grid code, I have designed the following experiment. First, I model a case of a flat interface (Figure 1a). For this type of model no stair-step approximation needs to be made, therefore a regular finite-difference technique should give accurate results. The depth to the interface is 800 m, and the source is located 120 m above the interface. The P and S velocities and densities of the two layers are given in the figure. A snapshot computed with finite differences for the model in Figure 1a is shown in Figure 2a. The snapshot shows the horizontal component of particle velocity (i.e., the component parallel to the interface) for a point-force source oriented vertically (perpendicular to the interface). The source signal is a Ricker wavelet with a center frequency of 20 Hz. The snapshot is taken at a time of 0.2 s. Next, I rotate the whole experiment by 30° (Figure 1b), i.e., I rotate the interface, and the source orientation. The source is therefore still oriented perpendicular to the interface. For this model I now compute snapshots of the particle velocity component parallel to the interface. Thus, with the exception of the effects from the free surface and (imperfectly) absorbing boundaries, the snapshots computed for the tilted model should look like those computed for the flat model, but rotated by 30°. Figure 2b shows the result computed with the finite-difference scheme, while Figure 3b shows the irregular-grid result. In the irregular-grid computation, the grid has been distorted in such a way that particle-velocity grid points lie exactly on the dipping interfaces. Figure 3a is the same as Figure 2a. It is shown here again in order to facilitate the comparison.

Comparison of Figure 2b with Figure 2a shows that while the overall appearance of the snapshots is still similar some noticeable differences are observed particularly in the region (marked by a circle in Figure 2b where several waves (the direct S wave, the reflected S wave, and the P to S converted wave) interfere, and where a critical angle for the reflected S is present. The amplitude-versus-angle behavior of the waves reflected at the sloping interface in no longer modeled accurately. Comparison of Figure 3a with Figure 3b, on the other hand, shows that the accuracy of the amplitude-versus-angle behavior for the tilted interface has improved considerably. Figure 3b is more or less a tilted version of Figure 3a.

This comparison demonstrates that, as expected, the irregular-grid method can model irregular interfaces more accurately than a standard finite-difference scheme.

A FREE-SURFACE EXAMPLE

As the irregular-grid technique is able to handle irregular solid-solid interfaces, it can be applied with confidence to an irregular free surface. This is because, as mentioned above, the method treats the free surface the same way as any other interface. To demonstrate this capability, I now apply it to a model with irregular surface topography, where the grid is computed in such a way that it lines up with the surface.

First, Figure 4 shows an example of such a grid approximating a sloping surface. Note that only triangles with at least one of their vertices at the free surface are distorted. All other triangles are equilateral. For equilateral triangles my modeling scheme is of second-order accuracy. Otherwise the accuracy is first-order (Nolte, 1996). For the gridding used in Figure 4 and in the example below the accuracy is therefore second-order everywhere, except on the free surface where it is first-order. Also note that the grid has been computed in such a way that none of the distorted triangles have angles greater than 90°. This is desirable, as it facilitates computation of the area elements A and the polygons ∂A (see the appendix for the definition of these terms). The reason for this is that for triangles with angles $\leq 90°$ the circumcenter (the center of the circle through the vertices, see Figure A-2) is located within that triangle. A triangle with an obtuse angle, on the other hand, would have its circumcircle outside the triangle, which can be easily visualized from Figure A-2.

The model with irregular surface topography that is used for the computations below is shown in Figure 5. The horizontal length of the model is 2 km, the average vertical length is 1.1 km. The topographic relief is 200 m. A single reflecting interface is located at an average depth of 800 m (300 m from the bottom). The P and S velocities and the density are given in the figure.

Figure 6 shows a series of snapshot taken at time intervals of 0.05 s, starting at a time of 0.1 s. In this case the source was a vertically oriented point force, and the snapshots show the vertical component of particle velocity. The most prominent effect of the irregular surface topography is the presence of scattered surface waves, primarily from the peak at about a third of the horizontal model length from the left. These scattered waves can be seen best at the later times. As can be seen, both incident P waves and S waves cause these scattered waves.

DISCUSSION

The memory requirements of the technique have not been addressed thus far. As stated in Nolte (1996), the irregular grid requires more memory per grid point then a regular-grid method. The additional quantities that need to be stored for each grid point are its coordinates and the indices of its neighbors. Also, the total number of stress points will be larger than the total number of velocity points (the exact ratio of these two quantities depends on the grid irregularity). On the other hand, the method allows variable grid-point spacing, so that the spacing can be locally scaled to the medium

velocity as well as to the amount of detail with which one desires to model particular areas of a model. For example, for a model in which regions with strongly different velocities are present, the irregular-grid method would require fewer grid points than a second-order finite-difference program. Higher-order, finite-difference schemes, on the other hand, may still require fewer grid points in some cases, but they are even worse at accurately modeling irregular interfaces.

In many cases a hybrid method might be desirable. For example, the irregular-grid technique could be used only in the near surface region in order to take advantage of its accurate irregular-surface modeling capability. At greater depth a finite-difference may be sufficient and in some cases more efficient. This would suggest a coupling of the two methods. This can be implemented trivially in the SH case. In the P-SV case some of the stress points would need to be interpolated in order to couple the irregular-grid to a regular staggered grid. However, this interpolation can be easily done and is one of the planned future extensions of the method.

Another potential application area for the technique is the modeling of seismic wave propagation in the presence of boreholes. This is of particular interest for modeling the wave fields from downhole sources, for example in single-well or cross-well experiments. The flexibility in grid geometry allows to parameterize such models on a grid that is lined up with the borehole wall.

A potential extension of the code to 3-D is easy in principle. Taking the method to 3-D would require tetrahedral instead of triangular Delaunay cells. In practice, one of the main difficulties is the problem of the grid computation itself, i.e., fitting a tetrahedral grid to a model in such a way that it lines up with the interfaces and that the grid spacing is scaled to the medium velocities. However, the development of efficient 3-D gridding algorithms is an area of extensive research (e.g., the GOCAD Research Program), so that existing software can be used to perform this task.

There are also alternative ways to do the 3-D implementation. For example, if the objective is to simulate wave propagation for a model with a borehole it may be desirable to use prisms instead of tetrahedra as the basic grid cells, i.e., use irregular grids in the horizontal planes and regular grid spacing in the vertical direction. The details of such an approach still remain to be worked out, which is another task planned for the future.

CONCLUSIONS

In this paper I have demonstrated the ability of the irregular-grid technique to accurately model irregular interfaces. A comparison with a finite-difference technique showed that the irregular-grid method produced superior results, as no stair-step approximation to interfaces is made. I also showed the applicability of the method to an irregular free surface. A numerical test showed that surface irregularities gave rise to numerous scattered waves.

ACKNOWLEDGMENTS

This work was supported by the Reservoir Delineation Consortium at the Massachusetts Institute of Technology.

REFERENCES

Alford, R. M., Kelly, K. R., and Boore, D. M., 1974, Accuracy of finite-difference modeling of the acoustic wave equation, *Geophysics, 39*, 834–842.

Dirichlet, G. L., 1850, Über die Reduktion der positiven quadratischen Formen mit drei unbestimmten ganzen Zahlen, *J. Reine u. Angew. Math., 40*, 209–227.

Delaunay, B. N., 1934, Sur la sphere vide, *Bull. Acad. Science, USSR VII: Class. Sci. Math.*, 793–800.

De Lilla, A., 1997, Finite difference seismic wave propagation using variable grid sizes, *M.Sc. Thesis, Massachusetts Institute of Technology.*

Hestholm, S. O., 1996. 3-D finite-difference elastic wave modeling including surface topography, *66th Ann. Int. Mtg. Soc. Expl. Geophys., Expanded Abstracts*, 662–665.

Hestholm, S. O. and Ruud, B. O., 1994. 2-D finite-difference elastic wave modelling including surface topography, *Geophys. Prosp., 42*, 371–390.

Higdon, R. L., 1986, Absorbing boundary conditions for difference approximations to the multi-dimensional wave equation, *Math. Comp., 47*, 437–459.

Higdon, R. L., 1987, Numerical absorbing boundary conditions for the wave equation, *Math. Comp., 49*, 65–90.

Jastram, C. and Tessmer, E., 1994, Elastic modeling on a grid with vertically varying spacing, *Geophys. Prosp., 42*, 357–370.

Jih, R. S., McLaughlin, K. R., and Der, Z. A., 1988, Free-boundary conditions of arbitrary polygonal topography in a two-dimensional explicit elastic finite-difference scheme, *Geophysics, 53*, 1045–1055.

Levander, A. R., 1988, Fourth-order finite-difference P-SV seismograms, *Geophysics, 53*, 1425–1436.

Muir, F., Dellinger, J., Etgen, J., and Nichols, D., 1992, Modeling elastic wave fields across irregular boundaries, *Geophysics 57*, 1189–1193.

Nolte, B., 1996., Modeling of elastic wave propagation on irregular triangular grids using a finite-volume method, *Borehole Acoustics and Logging and Reservoir Delineation Consortia, Annual Report, Earth Resources Laboratory, M.I.T.* 10-1–10-20.

Robertsson, J. O. A., 1996 A numerical free-surface condition for elastic/viscoelastic finite-difference modeling in the presence of topography, *66th Ann. Int. Mtg. Soc. Expl. Geophys., Expanded Abstracts*, 670–673.

Robertsson, J. O. A., Levander, A., Symes, W. W., and Hollinger, K., 1995, A comparative study of free-surface boundary conditions for finite-difference simulation of elastic/viscoelastic wave propagation, *65th Ann. Int. Mtg. Soc. Expl. Geophys., Expanded Abstracts*, 1277–1280.

Tessmer, E., Kosloff, D., and Behle, A., 1992, Elastic wave propagation simulation in the presence of surface topography, *Geophys. J. Int., 108*, 621–632.

Vinokur, M., 1989, An analysis of finite-difference and finite-volume formulations of conservation laws, *J. Comp. Phys., 81*, 1–52.

Virieux, J., 1984, SH wave propagation in heterogeneous media: velocity-stress finite-difference method, *Geophysics, 49*, 1933–1957.

Virieux, J., 1986, P-SV wave propagation in heterogeneous media: velocity-stress finite-difference method, *Geophysics, 51*, 889–901.

Wang, Y. and Schuster, G. T., 1996, Finite-difference variable grid scheme for acoustic and elastic wave equation modeling, *66th Ann. Int. Mtg. Soc. Expl. Geophys., Expanded Abstracts*, 674–677.

APPENDIX

A more detailed description of the modeling technique is given in Nolte (1996). Here, I only give a brief review of the method for the P-SV case and correct some errors of the earlier paper.

Figure A-1 defines some terms used in the equations below. For an area A with boundary ∂A the normal to ∂A, I introduce local coordinates n and s, normal and tangential to ∂A, respectively. With ϕ denoting the angle between n and the Cartesian x direction, the local and Cartesian coordinates are related through:

$$\begin{aligned} n &= x\cos\phi + z\sin\phi \\ s &= -x\sin\phi + z\cos\phi \\ x &= n\cos\phi - s\sin\phi \\ z &= n\sin\phi + s\cos\phi \end{aligned} \tag{A-1}$$

Using the above definitions I write the wave equation in integral form as

$$\begin{aligned} \iint_A dA\,\rho\frac{\partial v_x}{\partial t} &= \oint_{\partial A} ds\,(\sigma_{nn}\cos\phi - \sigma_{ns}\sin\phi) \\ \iint_A dA\,\rho\frac{\partial v_z}{\partial t} &= \oint_{\partial A} ds\,(\sigma_{nn}\sin\phi + \sigma_{ns}\cos\phi). \end{aligned} \tag{A-2}$$

Here, v_x and v_z are the x and z components, respectively, of the particle velocity, while σ_{nn} and σ_{ns} are the normal and tangential stresses on ∂A.

The constitutive relation (Hooke's law) can be written as

$$\begin{aligned} \frac{\partial\sigma_{nn}}{\partial t} &= (\lambda+2\mu)(\frac{\partial v_x}{\partial n}\cos\phi + \frac{\partial v_z}{\partial n}\sin\phi) + \lambda(\frac{\partial v_z}{\partial s}\cos\phi - \frac{\partial v_x}{\partial s}\sin\phi) \\ \frac{\partial\sigma_{ns}}{\partial t} &= \mu\left[(\frac{\partial v_z}{\partial n} + \frac{\partial v_x}{\partial s})\cos\phi + (\frac{\partial v_z}{\partial s} - \frac{\partial v_x}{\partial n})\sin\phi\right]. \end{aligned} \tag{A-3}$$

In order to discretize these equations the model is parameterized using Delaunay and Dirichlet grids (Delaunay, 1934; Dirichlet, 1850) as illustrated in Figure A-2. A Delaunay grid is a triangular grid that connects nearest neighbors. This nearest-neighbor condition means that a circle through the three vertices of any triangle (a so-called *circumcircle*) does not enclose any other vertex. The corresponding Dirichlet grid is obtained by connecting the centers of the circumcircles (the *circumcenters*) of neighboring Delaunay triangles.

I now specify particle velocity at the Delaunay vertices, and use the area enclosed by the polygon around any particle-velocity point as the area A of Figure A-1 while I use the polygon itself as its boundary ∂A. I assume that the medium parameters (λ, μ, and ρ) as well as all stresses are constant within each Delaunay triangle.

The notations used are shown in Figure A-3a and A-3b. In Figure A-3b I have introduced the velocities v_1,v_2,v_3, and v_3, for convenience. As can be seen, v_3 is the velocity $v_{[j,k-1]}$, and v_2 is $v_{[j,k+1]}$; v_1 is interpolated from v_j, $v_{[j,k]}$, and v_2; v_4 is interpolated

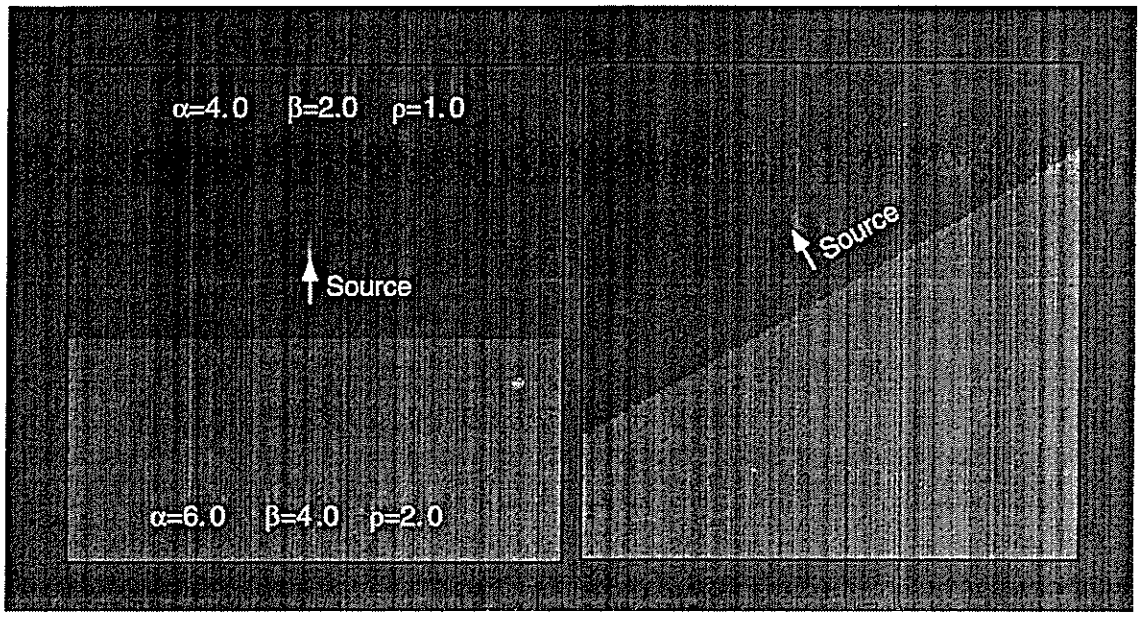

Figure 1: Models used for comparing the irregular-grid method with finite differences. The P and S velocities (in $\mathrm{km\,s^{-1}}$) and densities (in $\mathrm{g\,cm^{-3}}$) are given in the figure. (a) A flat interface is located at a depth of 800 m. The source is a point force located 120 m above the interface. The source orientation is perpendicular to the interface as indicated by an arrow in the figure. (b) The experiment is rotated by 30°. The source orientation is again indicated by an arrow in the picture.

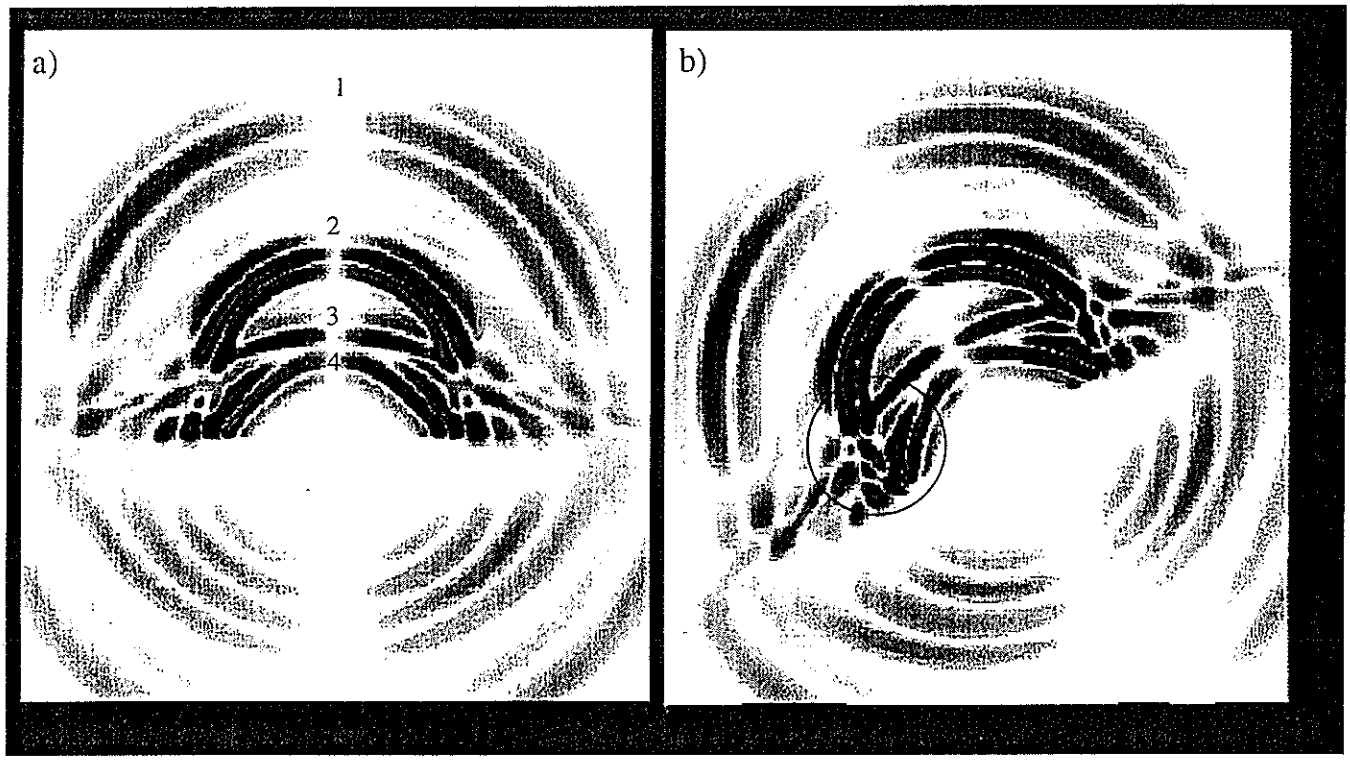

Figure 2: Snapshots computed with finite differences for (a) the model of Figure 1a and (b) the model of Figure 1b. The snapshots show the component of particle velocity parallel to the interface at the time of 0.2 s. The waves identified in (a) are the direct P wave (1), the direct S wave (2), the P-to-S converted wave (3), and the reflected S wave (4). The region enclosed by the circle in (b) is inaccurately modeled with finite differences.

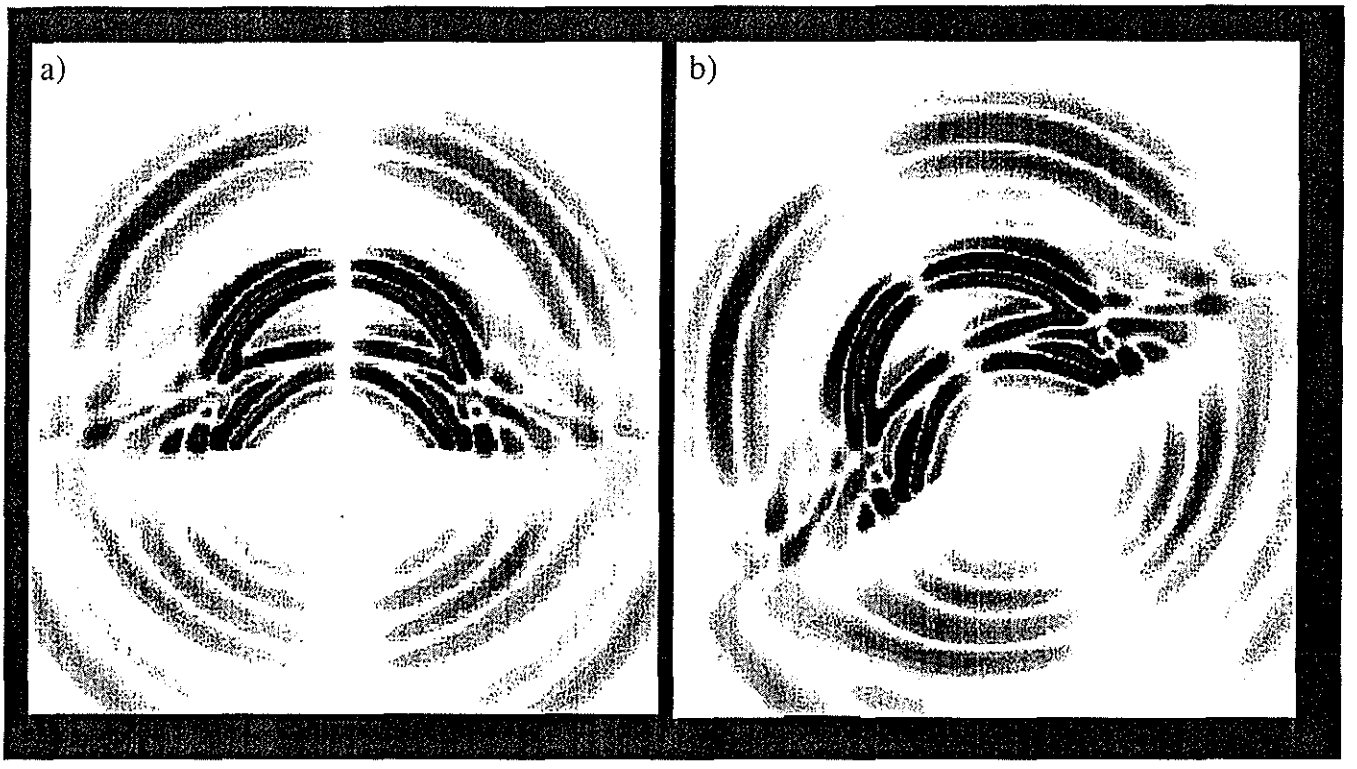

Figure 3: Same as Figure 2, but showing the snapshot computed with the irregular-grid method (b) for the tilted-interface model. Note the improved accuracy, particularly in the region where the finite-differences results were inaccurate (the region circled in Figure 2b.

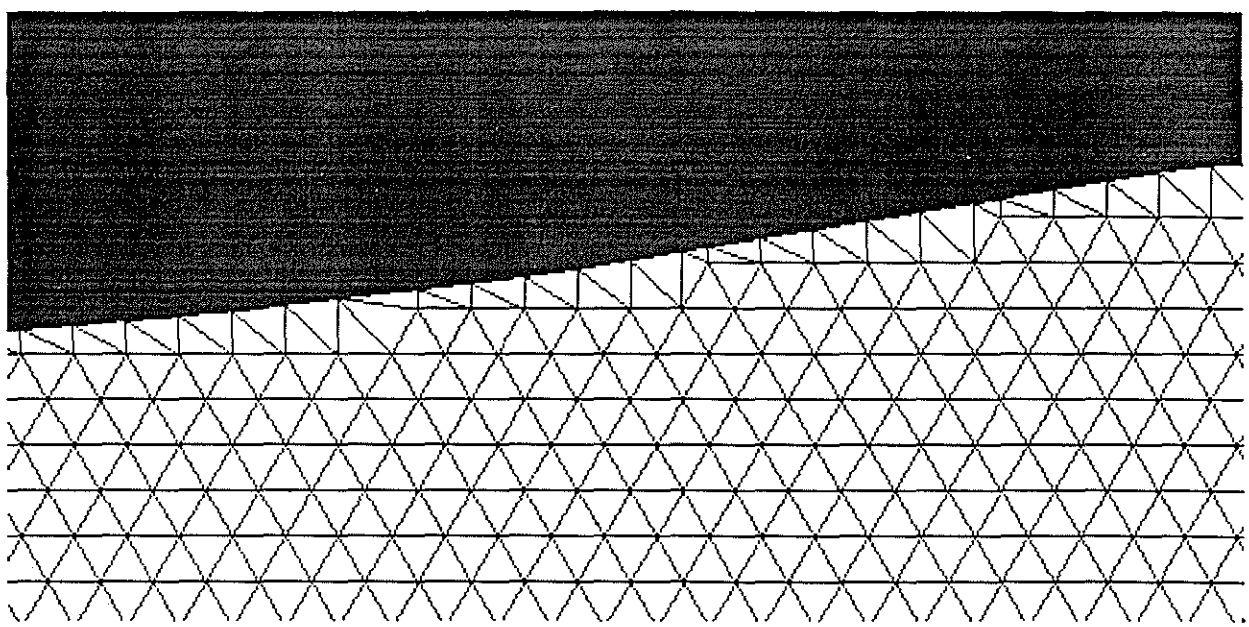

Figure 4: Example of a triangular grid that is lined up with an irregular free surface. All triangles except those that touch the free surface are equilateral. No angles greater than 90° are present anywhere in the grid.

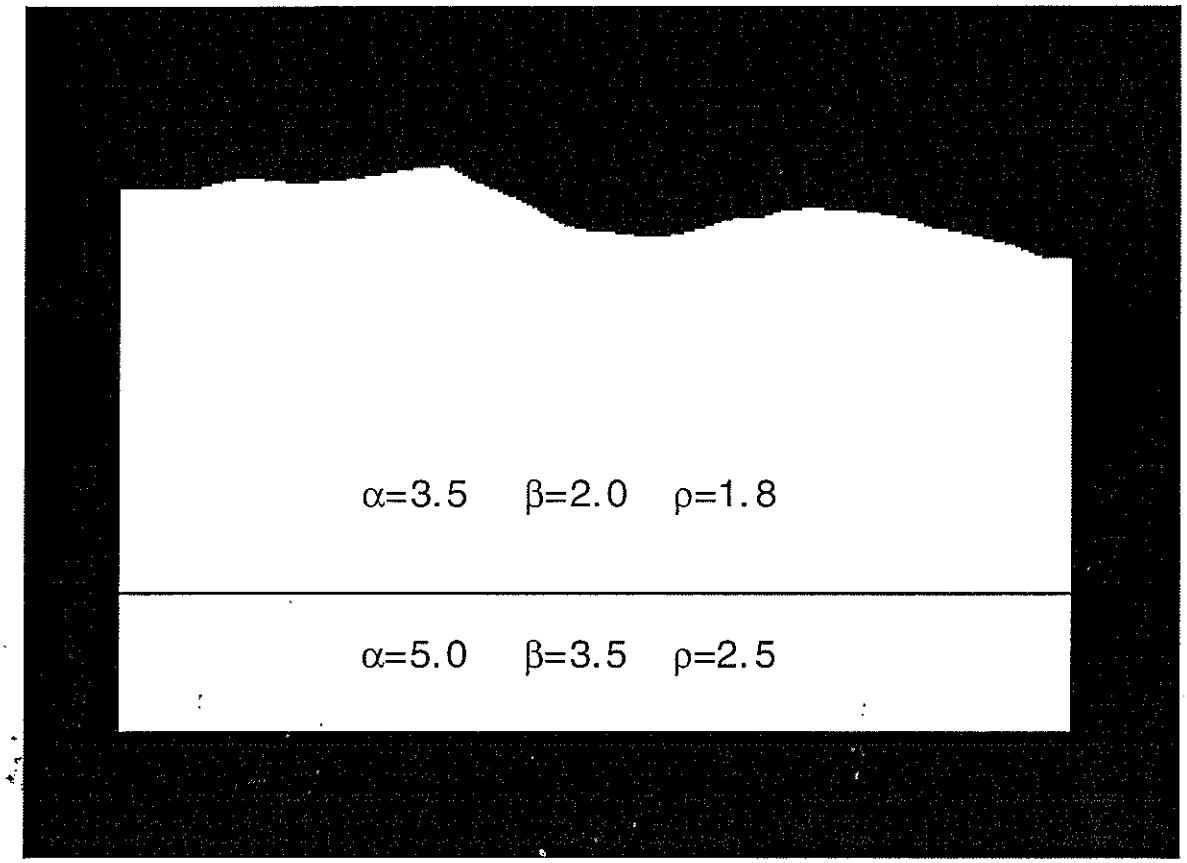

Figure 5: Model with irregular topography. The P and S velocities (in $\mathrm{km\,s^{-1}}$) and densities (in $\mathrm{g\,cm^{-3}}$) are given in the figure. The length of the model is 2 km, its height varies between 1 km and 1.2 km. This model is the input for the snapshots of Figure 6.

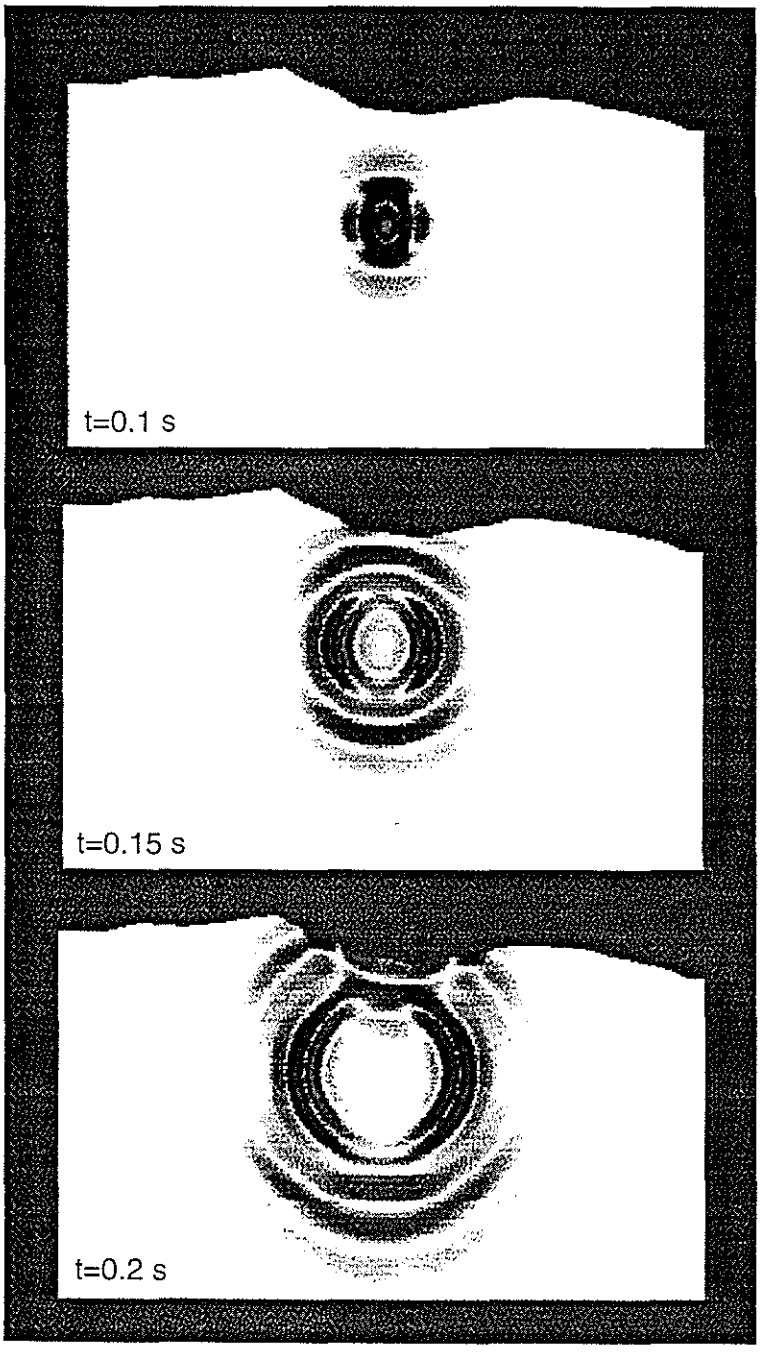

Figure 6: Snapshots computed for the model in Figure 5. The snapshots show the vertical component of particle velocity for at time intervals of 0.05 s, starting at 0.1 s. The source is a vertical point force.

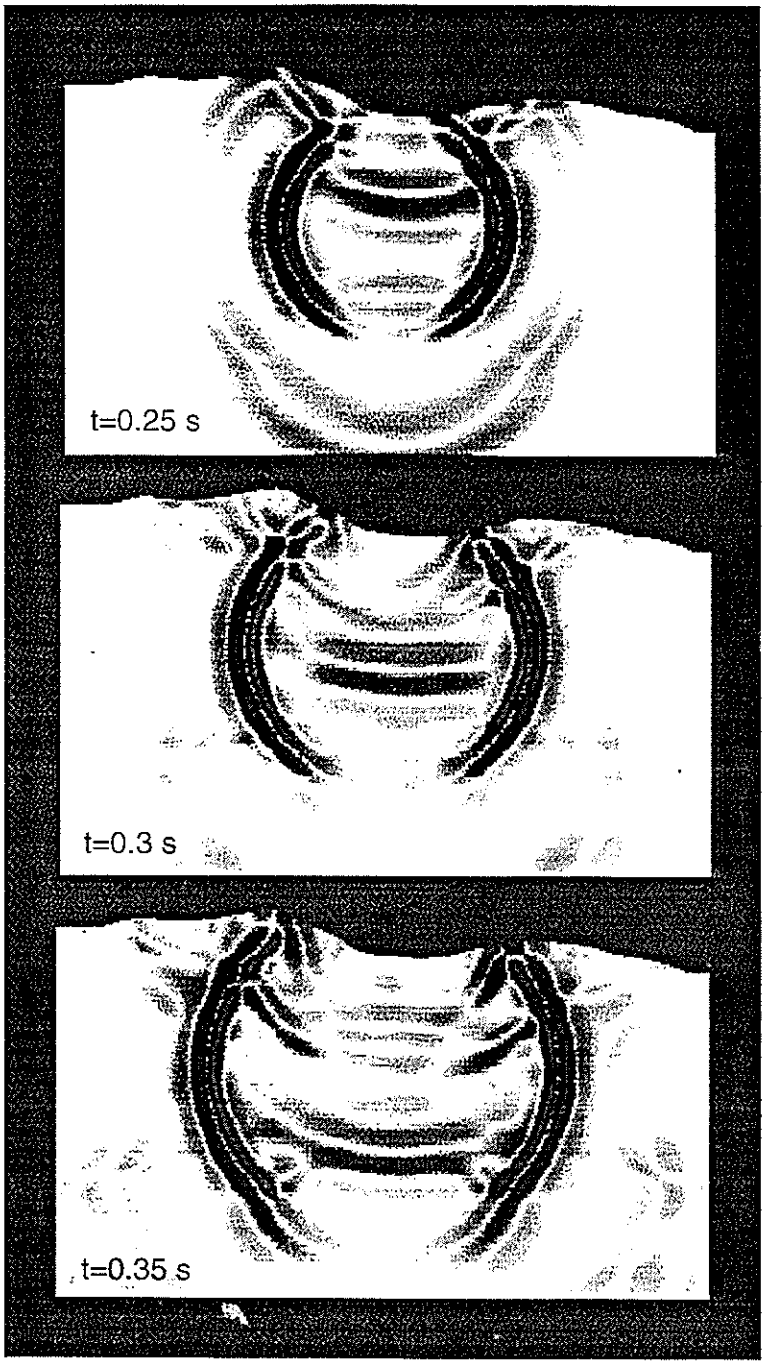

Figure 6, continued:

Figure 6, continued:

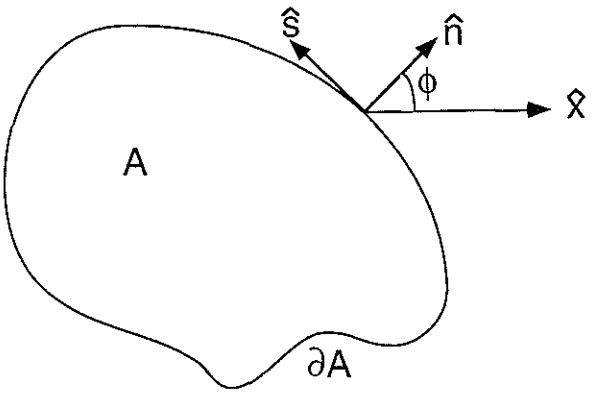

A-1: Definition of the area A, its boundary ∂A, the local coordinates n and s, and the angle ϕ used in the equations in the appendix.

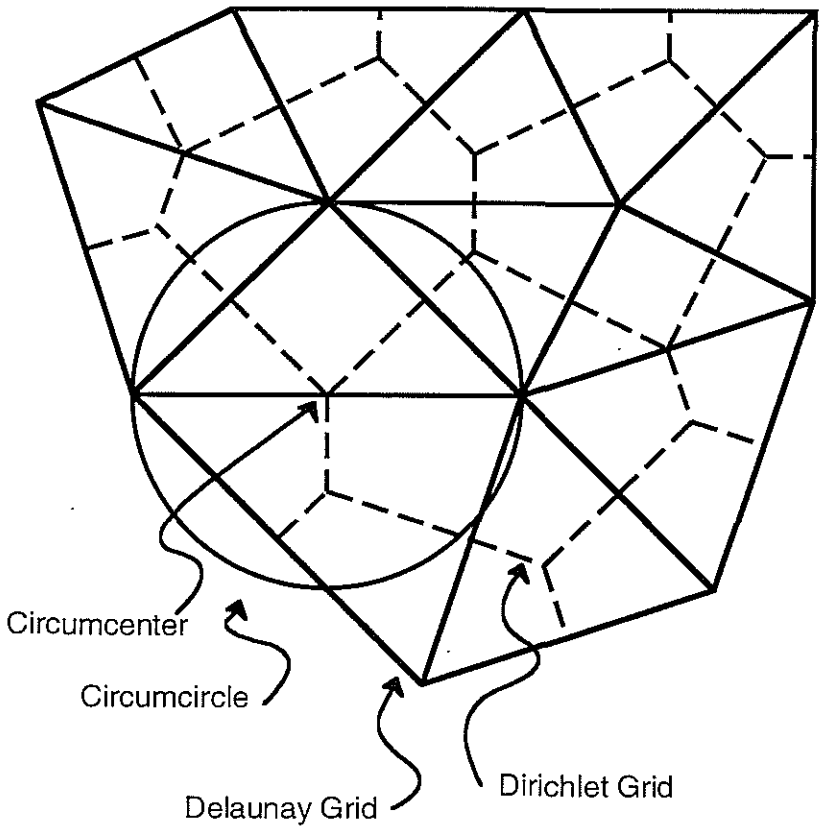

A-2: Schematic of a Delaunay grid and its dual Dirichlet grid. The circumcircle through the vertices of any Delaunay triangle does not contain any other triangle vertices. The circumcenters are the vertices of the Dirichlet grid.

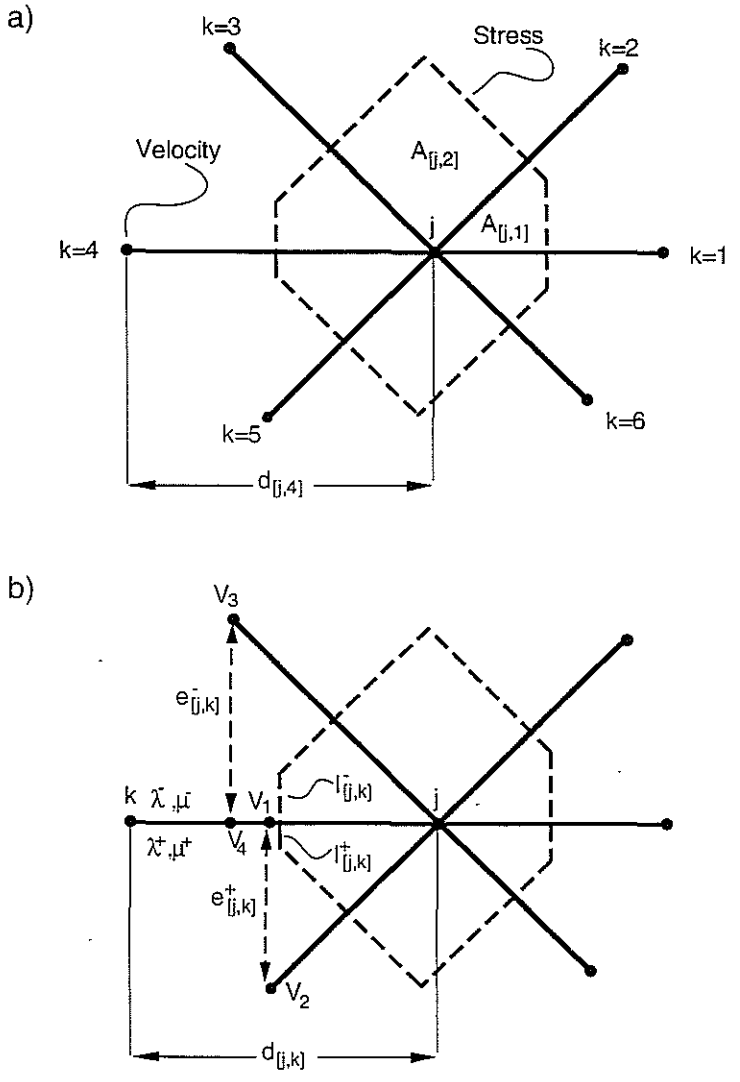

A-3: Sketch of the terms used in the discrete equations. (a) A particle-velocity point j with six neighbors k is shown. Stress is integrated over the dashed polygon. $A_{[j,k]}$ is an area element, and $d_{[j,k]}$ is the distance from point j to neighbor k. (b) Line segments $l_{[j,k]}$ over which stress is summed; velocity points v_1,v_2,v_3, and v_4 and lengths $e_{[j,k]}$ used for the computation of tangential velocity differences.